


The temperature of the WNM in the Milky Way

Nissim Kanekar¹ , Ravi Subrahmanyan², Jayaram N Chengalur³, Vicky Safouris⁴

¹ Kapteyn Institute, University of Groningen, Post Bag 800, 9700 AV Groningen

² Australia Telescope National Facility, CSIRO, Locked bag 194, Narrabri, NSW 2390, Australia

³ National Centre for Radio Astrophysics, Post Bag 3, Ganeshkhind, Pune 411 007

⁴ Dept. of Physics, University of Sydney, NSW 2006, Australia

Received mmdyy/ accepted mmdyy

ABSTRACT

We report high spectral resolution Australia Telescope Compact Array HI 21 cm observations resulting in the detection of the warm neutral medium (WNM) of the Galaxy in absorption against two extragalactic radio sources, PKS 1814–637 and PKS 0407–658. The two lines of sight were selected on the basis of the simplicity of their absorption profiles and the strength of the background sources; the high velocity resolution of the spectra then enabled us to estimate the kinetic temperatures of the absorbing gas by fitting multiple Gaussians to the absorption profiles. Four separate WNM components were detected toward the two sources, with peak optical depths $\tau_{\text{max}} = (1.0 \pm 0.08) \times 10^{-3}$, $(1.4 \pm 0.02) \times 10^{-3}$, $(2.2 \pm 0.05) \times 10^{-3}$ and $(3.4 \pm 0.05) \times 10^{-3}$ and kinetic temperatures $T_k = 3127 \pm 300$ K, 3694 ± 1595 K, 3500 ± 1354 K and 2165 ± 608 K respectively. All four components were thus found to have temperatures in the thermally unstable range $500 < T_k < 5000$ K; this suggests that thermal equilibrium has not been reached throughout the WNM.

Key words: radio lines: ISM – ISM: general – ISM: structure

1 INTRODUCTION

A corner stone of models for the Galactic interstellar medium (ISM) is that neutral hydrogen (HI) exists in two stable phases, in pressure equilibrium with one another (Field et al. 1969) and with the hot ionized medium (McKee & Ostriker 1977). Observationally, it has been established that HI indeed has two phases, (1) a cold dense phase (the cold neutral medium, CNM), which has high 21 cm optical depth and gives rise to the narrow absorption features seen toward continuum sources, and (2) a warm diffuse phase, the warm neutral medium (WNM) which contributes to the emission, but is extremely difficult to detect in absorption due to its low optical depth. Decades of study have established that the CNM has temperatures in the range 40 ± 200 K and number densities $n \approx 1 \pm 10$ cm^{−3} (e.g. Dickey, Terzian & Salpeter 1978; Payne, Salpeter & Terzian 1983; Heiles & Troland 2003a). On the other hand, while theoretical models (e.g. Wolfire et al. 1995) suggest that kinetic temperatures in the WNM lie in the range 5000 ± 8000 K, with number densities 0.01 ± 0.1 cm^{−3}, very little is as yet observationally known about physical conditions in this important constituent of the interstellar medium (e.g. Kulkarni & Heiles 1988).

Temperature measurements in HI clouds are usually carried out by comparing the 21 cm optical depth in a given direction (ob-

tained through 21 cm absorption studies toward background continuum sources) with the emission brightness temperature from nearby directions. This yields the excitation temperature of the HI gas, usually referred to as the “spin temperature”, T_s . In the CNM, T_s is driven toward the kinetic temperature T_k of the cloud, both by collisions and resonant scattering of Ly- α photons (Field 1958). Thus, for the CNM, 21 cm absorption/emission studies directly yield the kinetic temperature of an HI cloud or, in the case of multiple, blended, optically thin clouds along the line of sight, the column density weighted harmonic mean of the kinetic temperatures of the different clouds (e.g. Kulkarni & Heiles 1988). On the other hand, the temperature of the WNM is still weakly constrained due to the difficulties in detecting it in absorption (e.g. Mebold & Hills 1975; Kulkarni et al. 1985). Further, the particle and Ly- α number densities in the WNM may be too low to thermalize the hyperfine levels; T_s could hence be significantly lower than T_k here (Field 1958; Liszt 2001). 21 cm absorption/emission studies of WNM clouds thus provide a *lower* limit to the kinetic temperature, even in the rare cases of claimed detections of the WNM (e.g. Carilli, Dwarakanath & Goss 1998).

A serious problem with T_s measurements via the classical 21 cm absorption/emission studies is that such studies involve the comparison of the HI optical depth along a given line of sight with the brightness temperature obtained from other directions, i.e. the assumption that the HI cloud is uniform on scales much larger than the beam size. This is often untrue for the CNM and may well be incorrect for the WNM. Additionally, in cases where such stud-

[?] E-mail: nissim@astro.rug.nl (NK); rsubrahm@atnf.csiro.au (RS); chengalur@ncra.tifr.res.in (JNC); vickis@physics.usyd.edu.au (VS)

ies have been carried out with single-dish radio telescopes, the on-source absorption spectrum contains a contribution from HI emission in the beam; it is difficult to accurately correct for this effect. Single dish studies also require assumptions about the spatial distribution of HI clouds along the line of sight (which is unknown *a priori*), to correct for absorption of background HI emission by foreground CNM. Further, emission measurements suffer from the problem of stray radiation entering via the side-lobes of the telescope beam. Finally, searches for the WNM in absorption are usually confused by the multitude of CNM lines in any given direction, as even low column density CNM often has a higher optical depth than warm HI with a much higher column density.

We emphasize that it is the HI *emission* spectra which are most seriously affected by the above issues, stemming from stray radiation, non-uniformity of HI clouds across the beam, self-absorption, etc. These make it very difficult to estimate the spin temperature of the WNM in the standard absorption/emission searches. Conversely, HI absorption studies toward compact sources trace narrow lines of sight through the intervening clouds; when carried out using long baseline interferometers, these studies can resolve out the foreground HI emission (thus avoiding the above difficulties) and provide an uncontaminated measure of the absorption profile, which might then be inspected for WNM features. The only problems with such attempts to detect the WNM are that (1) the WNM optical depth is very low, i.e. high sensitivity is necessary to detect it in absorption, and (2) the WNM must be searched for in the midst of strong CNM absorption features. The latter issue can be mitigated by choosing lines of sight with simple CNM structure (with only a few narrow absorption components) and using high velocity resolution observations to model the deep narrow CNM features (e.g. as Gaussians) and subtract them out. One can then search for wide, shallow WNM absorption in the residuals and thus estimate (or constrain) the WNM temperature. Further, it is not necessary to know the spatial distributions of the absorbing clouds since optical depths are additive (for small τ) and the HI emission is resolved out. In fact, the WNM has indeed been detected by the above approach (albeit at cosmological distances), in the $z = 0.0912$ and $z = 0.2212$ damped Lyman- α systems toward QSO B0738+313. (Lane et al. 2000; Kanekar et al. 2001).

When the present observations were being planned, the Australia Telescope Compact Array (ATCA) was the only radio interferometer which could provide the requisite high velocity resolution ($\sim 0.5 \text{ km s}^{-1}$), along with large bandwidths to search for broad absorption. We hence carried out a pilot ATCA 21 cm absorption/emission survey toward a number of strong compact sources, to select those with the simplest absorption and emission profiles. Of these, PKS 0407-658 and PKS 1814-637 (Radhakrishnan et al. 1972) were chosen as the best candidates for a search for the WNM, both due to their high flux densities ($S_{20\text{cm}} \sim 15 \text{ Jy}$) and simple profiles. The ATCA observations and data analysis are described in Section 2 and the absorption spectra and Gaussian fits presented in Section 3.1; finally, implications for the temperatures in the absorbing HI clouds are discussed in Sections 3.2 and 3.3.

2 OBSERVATIONS AND DATA ANALYSIS

PKS 1814-637 and PKS 0407-658 were observed using the 6.0A array configuration of the ATCA in January 2001. This has a shortest baseline of 337 m, i.e. 1.7 k at the 21 cm line frequency, ensuring that foreground HI emission is resolved out and

does not affect the HI absorption spectrum. The system was configured to observe dual linear polarizations with a 4 MHz bandwidth covered by 2048 independent frequency channels; this provided a total velocity coverage of 844 km s^{-1} and a channel spacing of 0.4 km s^{-1} . Observations of PKS 1934-638 were used to calibrate the absolute flux density scale. The passband was calibrated through frequency switching every fifteen minutes on the target sources (which are themselves phase calibrators for the ATCA): the off-line scans were offset in frequency from the on-line ones by 10 MHz in order to implement the frequency switching purely as frequency changes in the first local oscillator, while maintaining the conversion chain electronics unchanged. This observing strategy was developed to obtain spectral baselines of high quality as the observations were aimed at detecting weak, broad spectral features. The total on-source, on-line time was five hours on each source.

The data were analyzed in MIRIAD. After the initial editing, gain and bandpass calibration and continuum subtraction, the data were shifted to the LSR velocity frame and spectral cubes were made from the continuum-subtracted visibilities. No absorption was detected toward other sources in the two fields; deconvolution was hence unnecessary and the final spectra toward the target sources were obtained by taking a cut through the cubes at the source positions. The flux densities of PKS 1814-637 and PKS 0407-658 were measured to be 14.38 Jy and 16.16 Jy respectively, while the spectra each have an RMS noise of 0.001 in units of optical depth (per 0.4 km s^{-1} spectral channel). The analysis was repeated after rejecting the shortest baseline (337 m), to test whether the spectra were at all affected by emission structure in this baseline; the shortest baseline in the remaining data was 628 m (i.e. 3.2 k). The spectra were found to be unchanged, apart from a marginal increase in the noise.

3 RESULTS AND DISCUSSION

3.1 Spectra

The final 0.4 km s^{-1} resolution absorption spectrum toward PKS 1814-637 is shown in Fig. 1(A) (solid points); here, optical depth is plotted against LSR velocity. For clarity, only the central 100 km s^{-1} of the spectrum are shown. Fig. 1(B) shows a zoomed-in version of this spectrum; shallow wide absorption can be clearly seen over the velocity range -10 to $+10 \text{ km s}^{-1}$. Since the deep narrow component is clearly asymmetric and there is additional broad absorption, we attempted to simultaneously fit three Gaussians to the absorption profile. This yielded an extremely stable, good fit, shown in Figs. 1(A) and (B) as a solid line. Attempts were also made to fit only two Gaussians to the profile but these were found to leave large residuals. Fig. 1(C) shows the spectrum after subtracting out the 3-component fit; the residuals are seen to lie within the noise. This residual spectrum was then smoothed to various velocity resolutions, up to a resolution of 35 km s^{-1} , to search for additional broad absorption; no new components were detected.

The absorption spectrum of PKS 0407-658, shown in Fig. 2(A), is far more complex than that of PKS 1814-637. Fig. 2(B) shows a zoomed-in version of the spectrum to emphasize the numerous absorption features spread over the range -30 to $+60 \text{ km s}^{-1}$; again, the solid points show the measured optical depth while the solid line shows our best multi-Gaussian fit. Wide, weak absorption features can again be seen in this spectrum, both at the base of the strong CNM components (velocity range: -15 to $+30 \text{ km s}^{-1}$) and, interestingly, at a location away from the central

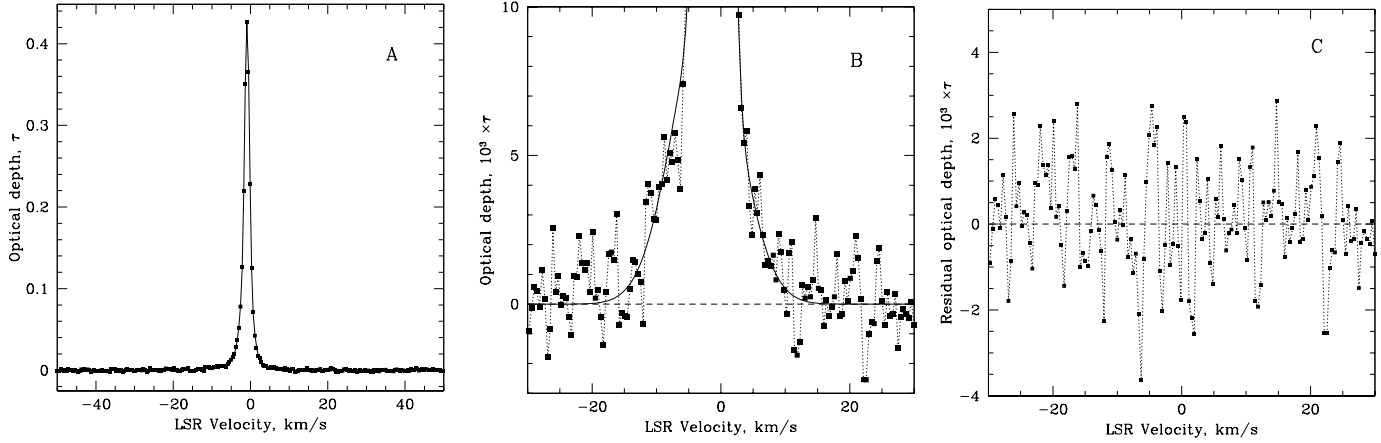


Figure 1. [A] : 0.4 km s^{-1} resolution absorption spectrum toward PKS 1814-637 (solid points), along with the 3-Gaussian fit (solid line). [B] : A zoomed-in version of this spectrum. A wide absorption component can be seen at the base of the narrow CNM features. [C] : The residual absorption spectrum after subtracting the fit; the residuals are seen to lie within the noise.

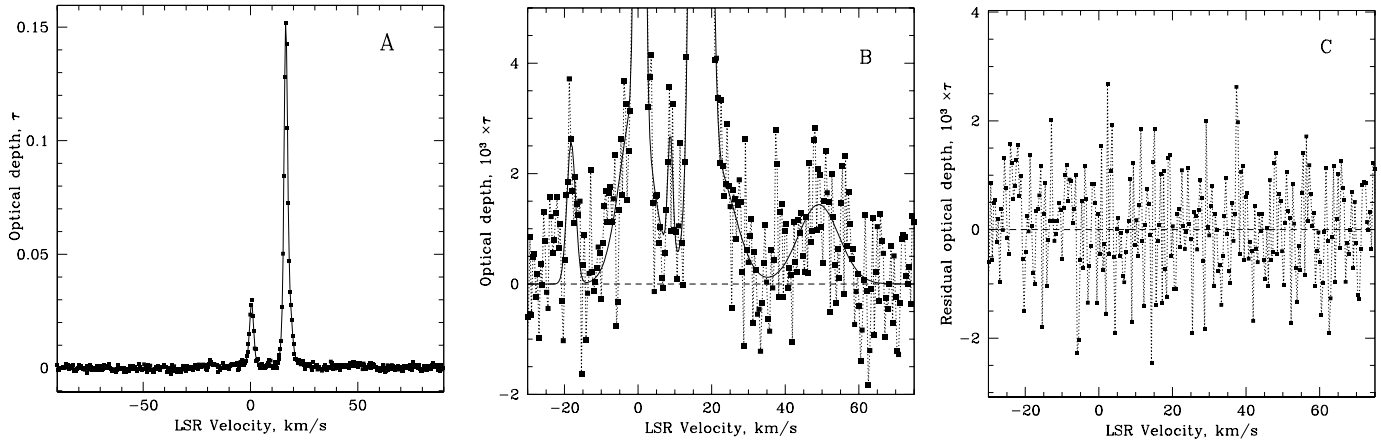


Figure 2. [A] : 0.4 km s^{-1} resolution absorption spectrum toward PKS 0407-658 (solid points), along with the 8-Gaussian fit (solid line). [B] : Zoomed-in version in which wide absorption can be seen at the base of the narrow CNM features as well as at an LSR velocity of $+49 \text{ km s}^{-1}$. [C] : The residual absorption spectrum after subtracting the fit; the residuals are seen to lie within the noise.

absorption complex, at an LSR velocity of $+49 \text{ km s}^{-1}$. Eight Gaussians were needed to obtain a good fit to the complex absorption profile. Attempts were again made to fit fewer Gaussians to the profile but these left large residuals in all cases. Fig. 2(C) shows the residuals after subtracting out the eight-Gaussian fit from the spectrum. These are seen to lie within the noise; no further components were detected on smoothing to coarser resolutions (up to 20 km s^{-1}). While the large number of components needed to obtain a good fit does raise questions about the uniqueness of the decomposition, the fit to the $+49 \text{ km s}^{-1}$ component is likely to be a good one as this is shifted in velocity relative to the main absorption components and the fit is thus only marginally affected by them.

3.2 HI kinetic temperatures

Table 3.2 lists the parameters of the multiple Gaussian fits to the two optical depth spectra. Here, Col. 3 gives the peak optical depth in each component, Col. 4, the velocity location of this peak and Col. 5, the FWHM of the component. The last two columns are the kinetic temperature and HI column density of the component,

obtained from the expressions $T_k = 21.855 \frac{V^2}{N_{\text{HI}}}$ and $N_{\text{HI}} = 1.823 \cdot 10^{18} \frac{T_k}{V}$, where V is the FWHM in km s^{-1} and we have used $dV = 1.06 \frac{V}{N_{\text{HI}}}$ (valid for a Gaussian) and assumed $T_s = T_k$. It should be emphasized that the above expression for N_{HI} is valid for the CNM but may not be valid for the WNM, where T_s may be lower than T_k (Liszt 2001); the quoted column densities for the WNM components should hence be viewed as upper limits. The above equations also assume that the observed velocity widths arise from Doppler broadening due to thermal motions; in the case of turbulent motions or blending of components, the values in Col. 6 and Col. 7 are upper limits on the true kinetic temperature and the HI column density.

In the case of PKS 1814-637, two of the three components have temperatures close to the known CNM range, with $T_{k1} = 44.6 \pm 0.7 \text{ K}$ and $T_{k2} = 248 \pm 10 \text{ K}$. The third component has a velocity width (FWHM) of 12.0 km s^{-1} , implying a kinetic temperature $T_{k3} = 3127 \pm 300 \text{ K}$. This lies significantly above the range of temperatures theoretically allowed for the CNM; however, it is below the canonical WNM range and in the thermally unstable range of temperatures $500 - 5000 \text{ K}$ (Wolfire et al. 1995). Thus, either

Table 1. Parameters of the simultaneous multiple Gaussian fits to the absorption spectra.

| Source | Component | Optical depth τ_{max} | | LSR velocity (km/s) | | FWHM (km/s) | | T_k K | | N_{HI} 10^{20} cm^{-2} | |
|--------------|-----------|--------------------------------------|--------|------------------------|-------|----------------|------|------------|------|--|------|
| PKS 1814 637 | 1 | 0:306 | 0:003 | 0:903 | 0:002 | 1:43 | 0:01 | 44:6 | 0:7 | 0:38 | 0:01 |
| | 2 | 0:110 | 0:003 | 1:05 | 0:01 | 3:37 | 0:06 | 248 | 10 | 1:77 | 0:15 |
| | 3 | 0:0099 | 0:0008 | 2:34 | 0:20 | 12:0 | 0:5 | 3127 | 300 | 7:2 | 1:7 |
| PKS 0407 658 | 1 | 0:111 | 0:002 | 16:394 | 0:008 | 1:73 | 0:03 | 65:7 | 2:1 | 0:24 | 0:02 |
| | 2 | 0:042 | 0:002 | 17:03 | 0:05 | 3:94 | 0:12 | 339 | 21 | 1:1 | 0:2 |
| | 3 | 0:0255 | 0:0007 | 0:51 | 0:03 | 2:11 | 0:08 | 97:2 | 7:2 | 0:10 | 0:02 |
| | 4 | 0:0014 | 0:0002 | 49:05 | 1:08 | 13:0 | 2:6 | 3694 | 1595 | 1:3 | 1:2 |
| | 5 | 0:0026 | 0:0005 | 18:18 | 0:28 | 2:8 | 0:7 | 165 | 88 | 0:02 | 0:03 |
| | 6 | 0:0034 | 0:0005 | 0:51 | 0:46 | 10:0 | 1:3 | 2165 | 608 | 1:4 | 0:9 |
| | 7 | 0:0022 | 0:0005 | 20:7 | 1:5 | 12:7 | 2:2 | 3500 | 1354 | 1:9 | 1:9 |
| | 8 | 0:0023 | 0:0007 | 8:75 | 0:25 | 1:6 | 0:6 | 59:3 | 54:7 | 0:04 | 0:13 |

HI indeed exists at thermally unstable temperatures in the Galaxy or the third component is due to non-thermally broadened CNM absorption. In the latter case, absorption by any WNM along this line of sight would be even weaker (and possibly broader) than this third component. However, after subtracting out the above three components and smoothing the spectrum to coarser resolutions, we find no evidence for any additional absorption. This non-detection places a 3 σ upper limit of $1.6 \times 10^{20} \text{ cm}^{-2}$ on the column density of HI gas at a *spin temperature* of 8000 K (i.e. with $T_k > 8000 \text{ K}$; Liszt (2001)). Note that this constraint on the column density is even stronger for a lower WNM spin temperature as the limit is directly proportional to T_s . If the third component is indeed non-thermally broadened CNM at a kinetic temperature T_{k3} , its column density is $N_3 = 0.23 \times 10^{20} T_{k3} \text{ cm}^{-2}$ (as $T_s = T_k$ for the CNM). Since $T_{k3} \lesssim 40 \text{ K}$ (Wolfire et al. 1995), the lower limit to the total CNM column density along this line of sight (from all three components) is $2.4 \times 10^{20} \text{ cm}^{-2}$. Combining this with the above upper limit on the WNM column density yields a 3 σ upper limit of $\sim 40\%$ on the fraction of HI along this line of sight that is in the WNM. This contrasts with the picture that the CNM and WNM are equitably distributed (e.g. Kulkarni & Heiles 1988; note that Heiles & Troland (2003b) find that as much as $\sim 60\%$ of all HI is in the WNM phase). Further, PKS 1814 637 is at a relatively high Galactic latitude; one would hence expect an even higher WNM fraction here than in lines of sight in the plane (e.g. Heiles & Troland 2003b), due to the lower pressure away from the plane (Wolfire et al. 1995). On the other hand, if the kinetic temperature is indeed $\sim 3127 \text{ K}$, the HI fraction in the WNM is $\sim 75\%$, as might be expected for a line of sight away from the plane. These arguments favour an interpretation where the third component arises in the WNM, with $T_{k3} = 3127 \text{ K}$, in the thermally unstable range.

Next, for PKS 0407 658, five of the Gaussian components in Table 3.2 are CNM, with temperatures in the range $T_k = 60 - 340 \text{ K}$. The remaining three components have kinetic temperatures $T_k = 2100 - 3700 \text{ K}$ and in the thermally unstable range. Two of these three wide components (#6 and #7, at LSR velocities 0.5 and 20.7 km s^{-1} respectively) lie within the velocity range of CNM absorption; consequently, the fits to these components might be confused by the CNM features. Component #4 (at $V_{\text{LSR}} = 49 \text{ km s}^{-1}$) is, however, some distance away from the central absorption complex; the fit to this component is thus likely to be unique. The temperature of this component is estimated to be $T_k = 3694 - 1595 \text{ K}$, from its velocity width. The errors on the fit are somewhat larger than that toward PKS 1814 637, due to

the complexity of the absorption spectrum and, consequently, the number of components needed to obtain a good fit. Unlike the case of PKS 1814 637, it is difficult to constrain the WNM column density along this line of sight — by adopting the hypothesis that all the wide absorption components are non-thermally broadened CNM — due to the possibility that a broad warm component might be lost in the welter of features in the central absorption complex.

It would be interesting to estimate spin temperatures by the “classical” method and to compare them to the kinetic temperatures of Table 3.2. One could also use the absorption fits to “predict” the emission profile and compare this to the observed emission. While both of these would serve as cross-checks to the derived parameters, one should note that modelling the emission profile requires additional assumptions about the distribution of the CNM and WNM along the line of sight. This is especially critical for velocity regions containing multiple components, such as the central absorption complex towards PKS 0407 658. Next, while the present observations also allowed us to measure the HI emission profiles along the two lines of sight, the large primary beam of the 22m ATCA dishes imply that these spectra are very likely to be affected by the issues discussed in Section 1. With this caveat in mind, we will use the present spectra for a brief comparison between T_s and T_k and the predicted and observed emission profiles. In the case of the $+49 \text{ km s}^{-1}$ component towards PKS 0407 658, reasonable agreement can be obtained between the predicted and observed emission if we assume $T_s = 1400 \text{ K}$, i.e. a factor of 2.5 less than the kinetic temperature. Unfortunately, the large errors on T_k imply that this estimate of T_s is, in fact, within 1.5 of the kinetic temperature; the above comparisons are thus not very meaningful along this line of sight. We note, further, that our ATCA emission spectrum toward PKS 0407 658 shows about twice the brightness temperature seen in the Parkes spectrum of Radhakrishnan et al. (1972); this suggests that the HI has structure within the primary beam of the AT dishes, making a comparison between the observed and derived emission profiles unreliable. Observations are presently being carried out to obtain HI emission mosaics in the vicinity of both sources, with both high spatial and spectral resolution; these will be used to redo the above comparisons in detail. We hence defer a full comparison along this line of sight until these mosaic images are available. On the other hand, in the case of the relatively simple line of sight toward PKS 1814 637, T_s is found to be in reasonable agreement with T_k , apart from the velocity range -6 to $+3 \text{ km/s}$ where CNM absorption contributes significantly to the absorption profile (and thus lowers the spin tem-

perature). This supports the argument that the third absorption component indeed arises in the WNM. It is also interesting to note that the estimated T_s values are, in general, again somewhat *lower* than the kinetic temperature $T_k = 3127 \pm 300$ K. On the other hand, the predicted emission profile (assuming no absorption of background emission by cold foreground HI) has a higher peak brightness temperature than that observed in our ATCA spectrum by about a factor of three; the observed emission spectrum also has wider wings than the model emission profile. It is, at present, unclear if this is due to a significantly warmer undetected WNM phase (with $T_k \sim 10^4$ K) or because of the low angular resolution of the emission profile or emission-related issues. We note, finally, that it is possible to obtain a far better agreement between the predicted and observed emission profiles by leaving the WNM spin temperature and the amount of absorption of background emission by foreground CNM as free parameters. However, we again defer a full analysis till the mosaic emission profiles are available.

3.3 Discussion

In recent times, deep searches have been carried out for the WNM using both interferometers (Carilli et al. 1998; Dwarakanath et al. 2002) and single dishes (Heiles & Troland 2003a,b), again via a comparison between absorption and emission spectra. Carilli et al. (1998) used the Westerbork Synthesis Radio Telescope (WSRT) to detect weak ($\sim 10^{-3}$) broad absorption toward Cygnus A, blended with numerous, much deeper CNM features. They identified the broad component with the WNM, obtaining $T_s \sim 6000$ – 1700 K and $T_s \sim 4800$ – 1600 K in two velocity ranges (in broad agreement with the earlier single-dish results of Mebold & Hills (1975) and Kalberla et al. (1980)). Similarly, Dwarakanath et al. (2002) detected wide absorption toward 3C147 with the WSRT and estimated $T_s \sim 3600$ – 360 K. However, both these studies could be affected by the problems of comparing on-source absorption spectra with off-source emission. The observations also had relatively poor velocity resolution ($\sim 2 \pm 1$ km s $^{-1}$), allowing the possibility that the observed broad absorption is a blend of narrow CNM lines. It should be emphasized that these studies yielded estimates of the WNM *spin* temperature, which, as discussed earlier, may be lower than the kinetic temperature.

On the other hand, Heiles & Troland (2003a,b) used the Arecibo Telescope to carry out high velocity resolution (~ 0.4 km s $^{-1}$) 21 cm absorption/emission studies toward a number of compact radio sources; the high spectral resolution allowed them to fit Gaussians to the narrow CNM absorption features and to then model the emission spectra as a sum of the CNM Gaussians and additional Gaussians from the WNM. A least-squares fit to the emission spectra was then used to estimate the *kinetic* temperature of WNM components. A substantial fraction ($\sim 48\%$) of the WNM was found to be in the thermally unstable phase, with kinetic temperatures in the range 500 – 5000 K. While these results are exceedingly interesting, the observations were single-dish ones and hence subject to the problems discussed earlier. Attempts were made to correct for some of these issues by (1) using a grid of off-source pointings to better constrain the on-source emission spectrum by estimating the spatial derivatives of the brightness temperature in different directions and (2) including the effects of self-absorption in the least-squares fit. As the authors mention, the latter was indeterminate in most cases and it was hence only possible to distinguish between extreme situations. The effect of this uncertainty on their results is not well understood.

The present approach essentially combines the good features

of both the above methods, using high spectral resolution and interferometric baselines; the crucial difference is that we work entirely with the absorption spectra and are thus not affected by emission-related issues. The critical assumption involved in our analysis is the decomposition of the absorption profiles into thermally broadened Gaussians. If this assumption breaks down (e.g. due to blending of narrower components), our estimates provide upper limits on the kinetic temperature for the different components.

Wide absorption was detected along both lines of sight discussed here, with four components showing kinetic temperatures in the thermally unstable range $2000 < T_k < 5000$ K. The results appear quite robust for the line of sight toward PKS 1814–637, due to the relative simplicity of the absorption profile. Similarly, while the fits to the two central wide components (#6 and #7 in Table 3.2) toward PKS 0407–658 may not be unique, the component at $+49$ km s $^{-1}$ LSR velocity appears to be well fit by a single Gaussian. There is also no evidence suggesting that the four wide components are non-thermally broadened CNM; moreover, in the case of PKS 1814–637, the deduced CNM fraction and spin temperatures support the case that the wide absorption arises from the WNM. It thus appears that there do exist WNM components with kinetic temperatures in the thermally unstable range, in agreement with the earlier results of Heiles & Troland (2003a,b). This indicates that thermal equilibrium has not been reached throughout the WNM, possibly due to the low number densities here and hence the long time-scales needed to reach equilibrium (e.g. Wolfire et al. 2003). New and upgraded radio interferometers such as the ATCA, the WSRT and the Giant Metrewave Radio Telescope will allow this hypothesis to be tested on a statistically significant number of lines of sight in the Galaxy, thus enabling us to arrive at a better understanding of this important phase of the interstellar medium.

Acknowledgments The Australia Telescope is funded by the Commonwealth of Australia for operation as a National Facility managed by CSIRO.

REFERENCES

- Carilli C. L., Dwarakanath K., Goss W. M., 1998, *ApJ*, 502, L79
- Dickey J. M., Terzian Y., Salpeter E. E., 1978, *ApJS*, 36, 77
- Dwarakanath K., Carilli C. L., Goss W. M., 2002, *ApJ*, 567, 940
- Field G. B., 1958, *Proc. IRE*, 46, 240
- Field G. B., Goldsmith D. W., Habing H. J., 1969, *ApJ*, 155, L149
- Heiles C., Troland T., 2003a, *ApJS*, 145, 329
- Heiles C., Troland T., 2003b, *ApJ*, 586, 1067
- Kalberla P. M. W., Mebold U., Reich W., 1980, *A&A*, 82, 275
- Kanekar N., Ghosh T., Chengalur J. N., 2001, *A&A*, 373, 394
- Kulkarni S., Heiles C., Turner K., Dickey J., 1985, *ApJS*, 57, 631
- Kulkarni S. R., Heiles C., 1988, in *Galactic and Extra-Galactic Radio Astronomy* (2nd edition), G. Verschuur & K. I. Keller-mann eds., Springer-Verlag, 95
- Lane W., Briggs F. H., Smette A., 2000, *ApJ*, 532, 146
- Liszt H. S., 2001, *A&A*, 371, 698
- McKee C. F., Ostriker J. P., 1977, *ApJ*, 218, 148
- Mebold U., Hills D., 1975, *A&A*, 42, 187
- Payne H. E., Salpeter E. E., Terzian Y., 1983, *ApJ*, 272, 540
- Radhakrishnan V., Murray J. D., Lockhart P., Whittle R. P. J., 1972, *ApJS*, 24, 15
- Wolfire M. G., Hollenbach D., McKee C. F., Tielens A. G. G. M., Bakes E. L. O., 1995, *ApJ*, 443, 152
- Wolfire M. G., McKee C. F., Hollenbach D., Tielens A. G. G. M., Bakes E. L. O., 2003, *ApJ*, 587, 278